Unconventional mechanism of stabilization of a tetragonal phase in the perovskite ferroelectric $(PbTiO_3)_{1-x}(BiFeO_3)_x$

Rajeev Ranjan and K. Appala Raju
Department of Materials Engineering, Indian Institute of Science, Bangalore 560012, India
(Received 16 March 2010; revised manuscript received 18 June 2010; published 27 August 2010)

Temperature-dependent x-ray powder-diffraction study of the tetragonal compositions of $PbTiO_3$-$BiFeO_3$ series has revealed that, unlike for all the known ferroelectric perovskites, the compositions exhibiting giant tetragonality is stabilized from the cubic phase via a complex transition pathway which involve (i) formation of minor monoclinic phase with a large pseudotetragonality along with an intermediate tetragonal phase (major) with a small tetragonality, (ii) gradual vanishing of the intermediate tetragonal phase and concomitant increase in the monoclinic regions, and finally (iii) gradual transformation of the monoclinic phase to the tetragonal phase with giant tetragonality. The system seems to adopt such a complex transition pathway to create a microstructure with very large number of domains and interfaces for stress relief, which would not have been possible in case of a direct cubic-tetragonal transition.

DOI: 10.1103/PhysRevB.82.054119 PACS number(s): 77.80.B−, 61.66.Fn, 77.84.−s

I. INTRODUCTION

The perovskite ferroelectric $PbTiO_3$ (PT) has been at the center of many technological breakthroughs in the field of modern sensors/actuators, transducers, ferroelectric random access memories, etc.[1–3] The ground-state structure of PT is tetragonal (space group $P4mm$), which transforms from the cubic (space group $Pm3m$) phase due to condensation of a zone-center Γ_{15} soft mode below 490 °C.[4] The two other well-known perovskite ferroelectrics $BaTiO_3$ and $KNbO_3$ also exhibit similar cubic-tetragonal transition at 130 °C and 435 °C, respectively.[4] However, unlike PT, the ground-state structures of $BaTiO_3$ and $KNbO_3$ are rhombohedral (space group $R3m$).[4] It is a common observation that all perovskite ferroelectric compounds/solid solutions exhibiting tetragonal ($P4mm$) phase transform directly to the cubic (paraelectric) phase on heating in one-step process. That there can be exception to this "rule" has neither been suspected nor reported in literature. In this paper, we show that exception to this well-known mechanism occurs in ground-state tetragonal structures stabilized with an anomalously large (giant) tetragonality. The system investigated in this regard is the solid solution series $(1-x)PbTiO_3$-$(x)BiFeO_3$, which is well known for exhibiting giant tetragonality with increasing $BiFeO_3$ concentration in $PbTiO_3$.[5–11] The tetragonal spontaneous strain, traditionally defined as $c/a-1$, increases from 6% for pure $PbTiO_3$ to ~19% for $x=0.69$.[5,6,11] Such a dramatic increase in the tetragonal strain is not known in other ferroelectric systems amenable to synthesis under ambient pressure condition. The only two compounds which have been reported to exhibit a comparable tetragonality, $PbVO_3$ and $BiCoO_3$ ($c/a \sim 1.24$), could be synthesized only under high-pressure conditions.[12] It is demonstrated that the tetragonal structure with giant tetragonality observed at room temperature is not formed directly from the high-temperature cubic phase in a one-step transition process but evolves gradually from an intermediate monoclinic phase over a very large temperature interval 680–450 °C.

II. EXPERIMENTAL

Powders of $(1-x)PbTiO_3$-$(x)BiFeO_3$ were prepared by conventional oxide processing method using high purity (>99.5%) Bi_2O_3, Fe_2O_3, PbO, and TiO_2. The powders were first calcined at 800 °C for 2 h. Sintering was carried out at 1000 °C for 3 h in a covered alumina crucible with powders of the identical composition spread around to create the desired atmosphere to minimize volatilization of PbO and Bi_2O_3. It may be emphasized that after the sintering cycle the ceramic disks were found to be fragmented or develop cracks for compositions $0.00 \leq x < 0.50$. On the other hand sintered pellets (density~95%) could be obtained for the higher compositions. The reason for this anomalous sintering behavior is discussed later in this paper. For x-ray powder-diffraction experiments, the sintered specimens were crushed to fine powder and annealed at ~800 °C to remove residual stresses. High-temperature x-ray diffraction was carried out using Cu $K\alpha$ x-ray source on a Bruker powder diffractometer (model: D8 Advance). Rietveld analysis was carried out using the package FULLPROF.[13]

III. RESULTS AND DISCUSSION

A. Room-temperature structures

Figure 1 shows the composition evolution of the x-ray powder-diffraction patterns of $(1-x)PbTiO_3$-$(x)BiFeO_3$ at room temperature in two different limited 2θ ranges. The Bragg peaks in the patterns corresponding to $x=0.50$, 0.60, and 0.65 can be indexed with respect to the tetragonal cell of $PbTiO_3$ type. For $x=0.69$, two extra weak peaks can be seen at 22.4° and 32°. These correspond to 012 and 104/110 reflections (hexagonal indices) of the rhombohedral (space group $R3c$) phase of $BiFeO_3$ type. For $x=0.73$ the strongest peak correspond to the rhombohedral phase, suggesting rhombohedral phase to be the dominant phase for this composition and above. Interestingly, the 101 reflection of the tetragonal phase can still be seen in the pattern of $x=0.80$. This suggests that the two phases (rhombohedral +tetragonal) lie in the composition range $0.65 < x \leq 0.80$. A similar observation of extended phase coexistence has been reported recently by Zhu *et al.*[9] Based on a careful deconvolution of the x-ray diffraction Bragg peaks and magnetic

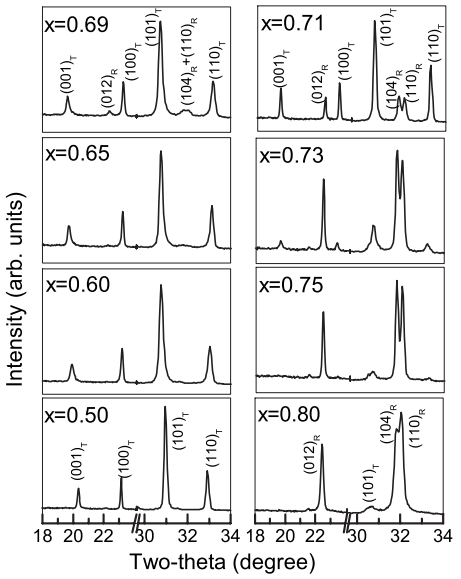

FIG. 1. X-ray powder-diffraction patterns in a limited 2θ region of $(1-x)PbTiO_3$-$xBiFeO_3$. The subscripts T and R with the indices represent peaks corresponding to the tetragonal and rhombohedral phases, respectively.

measurements, Zhu *et al.*[9] have also concluded about the presence of an orthorhombic phase in addition to the rhombohedral and tetragonal phases. In the previous studies the phase coexistence region has been reported for a narrower range $0.70 \leq x \leq 0.73$, presumably due to overlooking of the weak intensities of the Bragg peaks corresponding to the tetragonal and the rhombohedral phases, for compositions outside this narrow composition domain. In this paper we will be concerned about the structural phase transition behavior of only the tetragonal compositions $(0.00 \leq x < 0.69)$. Figure 2 shows composition dependence of the percentage spontaneous tetragonal strain defined as $100(c/a-1)$. In agreement with the previous results,[5,6,9,11] the tetragonality increases from 6% for $x=0.00$ to 19% for $x=0.71$. It is a well known fact that the large spontaneous strain associated with the paraelectric-ferroelectric phase transition of $PbTiO_3$ lead to fragmentation of the ceramic body as it is cooled through the Curie point. This is due to the fact that the large transformation stress buildup at the grain boundaries as the system transforms to the tetragonal phase on cooling below the Curie point disrupts the integrity of the grain boundaries already formed during the sintering process at high temperatures (1100 °C). Since the tetragonal strain increases with increasing $BiFeO_3$ concentration in $PbTiO_3$, in principle, none of the tetragonal compositions of $PbTiO_3$-$BiFeO_3$ should be sinterable under ordinary conditions. However, as mentioned in the experimental section, this was true only for compositions in the range $0.00 \leq x < 0.50$. For $x > 0.50$ we noticed improvement in the sinterability of the pellets (95% density) in spite of larger tetragonal strain. It is argued below that this improvement in the sinterability for compositions exhibiting giant tetragonality is intimately linked to the altered nature of the structural phase transition behavior of these compositions, a situation which has not been suspected in the literature of perovskite ferroelectrics.

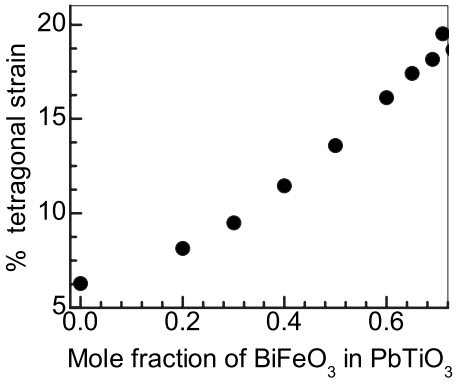

FIG. 2. Composition variation in the percentage tetragonality, $100(c/a-1)$.

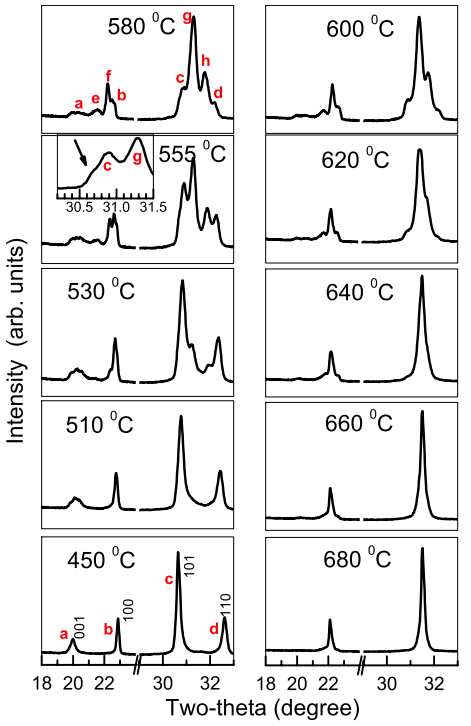

FIG. 3. (Color online) X-ray powder-diffraction patterns of $0.35PbTiO_3$-$0.65BiFeO_3$ at different temperatures in two different limited 2θ regions. The peaks a, b, c, and d correspond to the tetragonal phase at room temperature. The peaks labeled e, f, g, and h correspond to the newly formed (intermediate tetragonal) phase. The inset shows a magnified view of the Bragg profiles c and g. The arrow points to the shoulder in the peak c, which represents a monoclinic (Pm) distortion of the tetragonal cell.

B. Structural phase transition behavior of $x=0.65$

Figure 3 shows powder-diffraction patterns of $x=0.65$ in two limited 2θ regions around the 100 and 110 peaks at selected temperatures. The following features were worth noting in the pattern on increasing the temperature: (i) above 450 °C some of the tetragonal peaks, e.g., the 001 peak, start showing anomalous broadening, (ii) at 530 °C and above a set of new peaks (labeled as "e," "f," "g," and "h" in Fig. 3)

appear between the already existing tetragonal peaks (labeled as "a," "b," "c," and "d" in Fig. 3), the intensities of which grow with increasing temperature, (iii) the intensity of the peaks a, b, c, and d decreases on heating above 555 °C, without noticeable signature of the pairs a and b, and c and d approaching each other, which would have suggested a reduction in the tetragonality, and (iv) the pairs of the peaks e and f, and g and h tend to approach each other on heating, finally merging somewhere below 680 °C. A careful look of the pattern at 555 °C indicates that the intensity ratio of the pair of reflections e and f is nearly the same as that of a and b. Similarly, the intensity ratio of the peaks g and h is nearly the same as that of c and d. This suggests an almost one-to-one correspondence between the new peaks and the old peaks. The peaks e, f, g, and h therefore correspond to (001), (100), (101), and (110) planes, respectively, of a new intermediate tetragonal structure. This intermediate tetragonal phase has considerably reduced tetragonality (c/a) compared to the room-temperature tetragonal phase. At first glance, it gives an impression as if the system at 555 °C consists of two tetragonal phases, differing only in the lattice parameters. However, a careful examination of the profile shapes of the strong and relatively sharp peaks in the pattern revealed development of hump on the left of the peak c (see inset of Fig. 3) in the two phase region. This suggests a subtle structural distortion of the parent (low-temperature) tetragonal cell. Since a new Bragg peak could be seen without disappearance of any of the already existing tetragonal peaks, it is obvious that the parent tetragonal cell has undergone a symmetry lowering distortion at high temperatures. Also, since there was no evidence of appearance of new superlattice reflections at high temperatures in our case, we considered only the zone-center symmetry lowering distortions of the tetragonal cell. It may, however, be remarked that unlike electron diffraction,[8] x-ray diffraction is not a very sensitive technique for detection of weakly distorted superlattice phases. Based on the different low symmetry structural distortions reported for perovskite ferroelectric compounds/solid solutions, three simple low symmetry distortions were considered: (i) orthorhombic (space group *Bmm*2) type distortion similar to the 0 °C orthorhombic structure of the $BaTiO_3$,[14] (ii) monoclinic distortion of the *Cm* type reported for the morphotropic phase boundary compositions of $Pb(Zr,Ti)O_3$,[15] and (iii) monoclinic distortion of *Pm* type reported for $Pb(Mg_{1/3}Nb_{2/3})O_3$-$PbTiO_3$.[16]

To get an idea about the nature of splitting that would occur in the already existing tetragonal peaks as a result of these three types of distortion, x-ray powder-diffraction patterns for all the three types of distortions were simulated. Figure 4 shows the nature of the splitting developed in the 100/001 and 101/110 pairs of tetragonal reflections due to small distortions of the three types. It may be remarked that at the visual level the effect of varying the magnitude of the distortion (orthohombicity or monoclinicity) changes only the separation of the peaks. The intensity ratio of the peaks for a given distortion type was found to be not altered noticeably when the atomic positions were varied in conformity of the respective space groups. For instance, the nearly equal intensity seen in the doublet of the 101 reflection due to *Cm*-type distortion [Fig. 4(b)] was not affected to a noticeable degree before and after significant changes was made in the atomic positions of the *Cm* unit cell. It is evident from this figure that while no significant change is noticeable (at the visual level) in the 100/001 tetragonal reflections for all the three types of distortions, the 110/101 pairs do show visibly noticeable change. The *Pm*-type monoclinic distortion would split the 101 tetragonal peaks into three: one on the left and another on the right of the strongest reflection, each with nearly half the intensity of the strongest middle reflection. For the *Bmm*2-type distortion of the tetragonal cell, the (101) of the tetragonal remains a singlet while the 110 splits into two of nearly equal intensity [Fig. 4(a)]. A comparison of the three simulated patterns with observed profile shown in the inset of Fig. 3 suggests that the *Pm*-type distortion of the tetragonal cell is the most plausible among the three distortions considered above since the hump on the left of the peak c nearly matches the hump simulated in Fig. 4(c). The other hump expected on the right side of the strongest peak c will not be visible in the observed pattern because it would hidden between the peak c and the new peak g. In view of this analysis, the two phases coexisting at 555 °C has been proposed as monoclinic (*Pm*) and intermediate tetragonal (*P*4*mm*). The highly anisotropic peak broadening in the pattern was accounted by invoking the Stephen model incorporated within the FULLPROF package.[13] It was noted that the isotropic thermal parameters of Pb/Bi and Ti/Fe were very large for the intermediate tetragonal phase. As a result, we refined the anisotropic displacement parameters for these two atoms. Further, refinement of some of the atomic coordinates and thermal parameters of oxygen led to large oscillations in the refinement cycles, and hence such parameters were fixed. This is not very surprising in view of the fact that the quality of the XRD data deteriorated after the system entered into a two phase region, and that too with an intrinsic microstructure (probably very narrow-sized do-

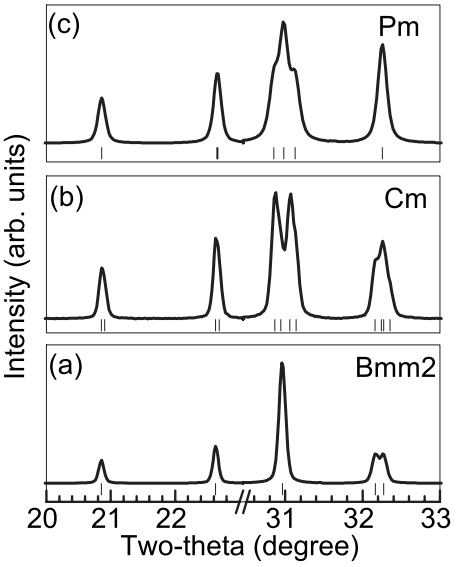

FIG. 4. Simulated x-ray powder-diffraction patterns near the 100/001 and 110/101 reflections of (a) orthorhombic *Bmm*2, (b) monoclinic *Cm*, and (c) monoclinic *Pm*-type distorted tetragonal cell.

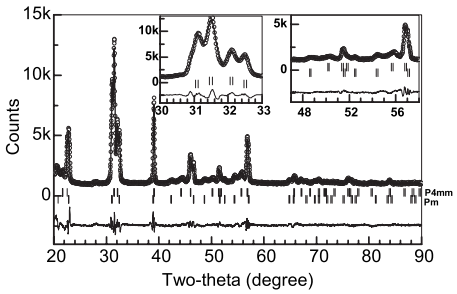

FIG. 5. Rietveld plot of 0.35PbTiO3-0.65BiFeO$_3$ at 555 °C. The fit was obtained after refinement with tetragonal($P4mm$) +monoclinic(Pm) two phase model. The upper and lower vertical bars represent calculated Bragg peak positions of the tetragonal and the monoclinic phases, respectively. The insets show magnified view in two different 2θ regions.

mains) which results in considerable peak broadening. Figure 5 shows the Rietveld fit of the 555 °C data using the proposed $Pm+P4mm$ phase model. The insets show magnified plot in two selected 2θ region of the pattern. It is evident that the calculated pattern fits reasonably well the observed pattern. The structural parameters of both the phases are shown in Table I. It is obvious from the refined parameter that the monoclinic distortion is small and, as anticipated from the analysis of the pattern, the metric of the monoclinic is pseudotetragonal with a very large pseudotetragonality ($c/a=1.096$). In fact, it was also possible to fit the diffraction pattern using two tetragonal phases. However, existence of two tetragonal structures differing only in their lattice parameters is a less likely possibility. A detailed neutron-diffraction

TABLE I. Refined structural parameters of monoclinic (Pm) and tetragonal ($P4mm$) phases of 0.65PbTiO$_3$-0.35BiFeO$_3$ at 555 °C. The isotropic and anisotropic thermal parameters are denoted by B and β_{ij}, respectively.

Phase: Monoclinic (Pm)				
Atom	x	y	z	B (Å^2)
Pb/Bi	0.00	0.00	0.00	1.6(1)
Ti/Fe	0.50	0.50	0.524(8)	0.5(3)
O1	0.50	0.50	0.00	1.0
O2	0.50	0.00	0.46(2)	1.0
O3	0.00	0.50	0.40(2)	1.0
$a=3.896(1)$ Å, $b=3.898(1)$ Å, $c=4.269(1)$ Å, $\beta=89.72°(7)$				
vol. fraction=35%				
Phase: Tetragonal ($P4mm$)				
Pb/Bi	0.00	0.00	0.00	$\beta_{11}=\beta_{22}=0.109(2)$, $\beta_{33}=0.093(3)$
Ti/Fe	0.50	0.50	0.524(8)	$\beta_{11}=\beta_{22}=0.054(4)$, $\beta_{33}=0.052(9)$
O1	0.50	0.50	0.05(2)	$B=1.0(7)$
O2	0.50	0.00	0.60(5)	$B=2.7(7)$
$a=3.947(1)$ Å, $c=4.099(1)$ Å, vol. fraction=65%				
$R_p=4.92$, $R_{wp}=7.29$, $R_{exp}=2.55$				

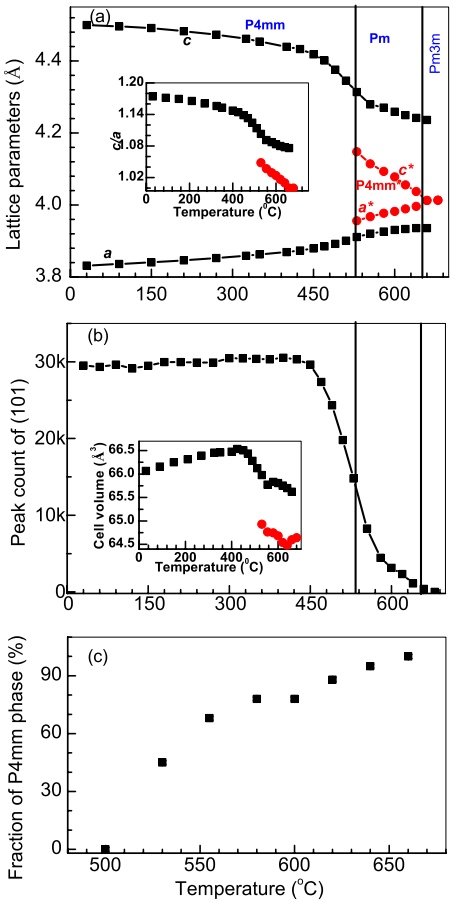

FIG. 6. (Color online) Temperature variation in the (a) lattice parameters, (b) peak count of the $(101)_T$ reflection, and (c) volume fraction of the intermediate tetragonal phase. For the monoclinic phase the pseudotetragonal lattice parameters are shown. $P4mm^*$ represents the high-temperature tetragonal phase (formed from the cubic phase). The inset in (a) shows the temperature variation in the tetragonality (pseudotetragonality for the monoclinic phase). The inset in (b) shows temperature variation in the cell volume of the different phases.

study may throw more light on the details of the structures of the proposed two phase model. It may be pointed that the lattice parameters of the orthorhombic phase postulated by Zhu *et al.*[9] for the compositions exhibiting phase coexistence at room temperature are also of the Pm-type cell. However, at present there does not seem to be any connection between these two low symmetry phases as the composition and temperature ranges in which they have been discovered are quite different. More detailed temperature-dependent study on different compositions of this system may throw more light on this issue.

Figure 6(a) shows temperature dependence of the lattice parameters of the different phases. It is interesting to note that even in the parent (low-temperature) tetragonal phase region, the c parameter decreases more abruptly after 450 °C. The same trend is evident in the temperature variation of the tetragonality, see inset of Fig. 6(a). The decrease in the tetragonality can be rationalized in terms of change in the polarization direction from [001] in the tetragonal phase to slightly away from the [001] direction in the a-c plane (as

allowed by the symmetry of the *Pm* space group) in the monoclinically distorted cell. Three other anomalous changes were also noted around this temperature: (i) sharp drop in the intensity of the strongest reflection, i.e., (101) after 450 °C [see Fig. 6(b)], (ii) change over from positive to negative volume thermal expansion behavior [see inset of Fig. 6(b)], and (iii) anomalous increase in broadening of some of the tetragonal reflection, e.g., the (001) reflection above this temperature. These observations suggests that although clear evidence of two phase (monoclinic +new tetragonal) could be seen at ~530 °C and above, the precursor effect associated with this transition sets in just above 450 °C. The anomalous broadening of the (001) peak suggests that the tetragonal (parent phase)—monoclinic transition is accompanied by formation of very small-sized (nano)domains along the [001] direction.

Viewed from the high-temperature side, the following picture emerges with regard to the transition pathway of this system: (i) the cubic phase transforms to an intermediate tetragonal phase, the tetragonality of which grows gradually with decreasing temperature, along with a minor monoclinic phase which has a large pseudotetragonality of 1.07, (ii) on lowering the temperature below 580 °C the monoclinic regions increase at the cost of the intermediate tetragonal regions and at ~510 °C the system is nearly single phase monoclinic (*Pm*) [see Fig. 6(c)], and (iii) the monoclinic phase gradually switchover to a high symmetry tetragonal phase in the temperature range 510–450 °C, which remains stable down to room temperature. Since the tetragonality of the intermediate tetragonal phase is very small just below 680 °C, and increases in a gradual manner, significant release of strain energy as a result of this particular transformation is not expected. On the other hand, the large pseudotetragonality ($c/a=1.07$) and cell volume (~1.5% larger than the cubic cell volume) of the minor monoclinic phase is likely to induce significant localized strains in the system. Since the order of the point groups $m3m$, $4mm$, and m corresponding to the cubic, tetragonal, and the monoclinic structures are 48, 8, and 2, respectively, a $m3m$ to $4mm$ transformation would lead to formation of six variants whereas a $m3m$ to m transformation would give rise to 24 variants. Thus, in principle, there is four times more number of variants available in the monoclinic structure than in the tetragonal phase. In addition, the monoclinic+tetragonal phase coexistence will also give rise to interfacial boundaries. From the above, it is obvious that in the two phase region, the system has large number of crystallographic domains and interfacial boundaries. The strain energy can therefore be distributed across such boundaries. Thus the complex microstructure resulting from such a transition pathway seems to provide a mechanism of stress relief in a gradual manner as the system evolves on cooling from the cubic phase. Had the tetragonal phase with giant tetragonality resulted from a direct cubic to tetragonal transition as in $PbTiO_3$, the corresponding large strain energy released could not possibly be accommodated by the system, leading to instability. Since the complex transition pathway provides a good mechanism of stress relief within the lattice itself, the grain boundaries in a ceramic body would experience less of the transformation stress. This would help retain the integrity of the grain boundaries as the ceramic is cooled after sintering and formation of pellets of good density could be possible. This explains the anomalous sintering behavior of this system mentioned in the experimental section.

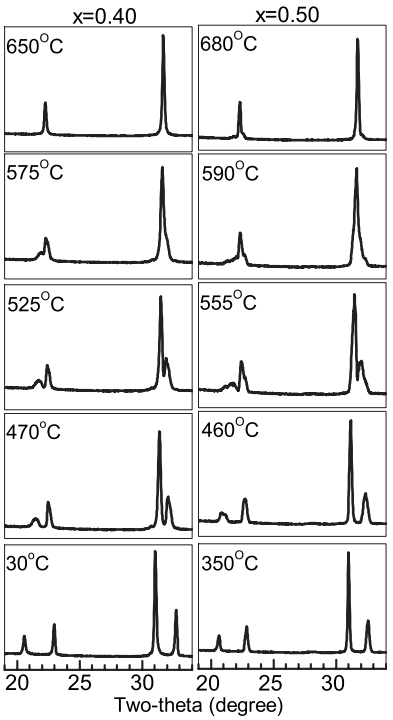

FIG. 7. Temperature evolution of the x-ray powder-diffraction patterns of $0.60PbTiO_3$-$0.40BiFeO_3$ (left column) and $0.50PbTiO_3$-$0.50BiFeO_3$ (right column) in a limited 2θ region.

C. Phase transition behavior of $x=0.40$ and $x=0.50$

For sake of comparison, we also investigated the phase transition behavior of two other compositions with lower $BiFeO_3$ concentration, i.e., $x=0.40$ and 0.50. The tetragonality of these compositions is 11.6% and 13.7%, respectively (see Fig. 2). Figure 7 shows the temperature evolution of the x-ray powder-diffraction patterns in a selected 2θ region of both the compositions. Unlike for the composition $x=0.65$, described above, there is no clear evidence of appearance of new Bragg peaks between the already existing tetragonal Bragg peaks. For both the compositions, the pair of peaks 001/100 and 101/110 approach each other with increasing temperature and finally merge. This is similar to what is anticipated for a direct tetragonal to cubic transition as in $PbTiO_3$. Interestingly, however, it may be noted that similar to the case of $x=0.65$, the 001 develops broadening at high temperatures (see the pattern corresponding to 470 °C of $x=0.40$ and 460 °C/555 °C of $x=0.50$ of Fig. 7). This suggest that although the overall phase transition behavior of $x=0.40$ and 0.50 is similar to that of $PbTiO_3$, both these compositions have a tendency to undergo the complex transition pathway exhibited by the composition $x=0.65$. In this context it is interesting note that broadening of 001 tetragonal peak is more for $x=0.50$ than $x=0.40$. This implies that, though not realized, the former has stronger tendency than

the later to exhibit the complex transition pathway. The compositions $x=0.40$ and 0.50, therefore seem to have two different types competing instabilities: (i) instability which lead to the direct cubic-tetragonal transition below a Curie point as in the parent compound $PbTiO_3$ and (ii) instability that leads to "complex" transition pathway as in the $x=0.65$ composition. Since the direct cubic-tetragonal transition in $PbTiO_3$ is driven by freezing of a zone-center Γ_{15} polar phonon mode, it may be argued that the occurrence of complex transition pathway is suggestive of the role of another factor at play. In this regard it may be emphasized that unlike $PbTiO_3$, the ferroelectric state in $BiFeO_3$ is not a result of condensation of a ferroelectric soft mode,[17] but is induced primarily by the lone $6s^2$ electron pair Bi^{+3} ions.[18] Hence with increasing concentration of $BiFeO_3$ in $PbTiO_3$, the $6s^2$ lone-pair electron induced ferroelectric distortion is likely to gradually dominate the system and suppress the ferroelectric soft mode.

IV. CONCLUSIONS

In conclusion, it is shown that the compositions exhibiting giant tetragonal strain of $\sim 19\%$ in the system $(1-x)PbTiO_3$-$(x)BiFeO_3$ does not follow the direct cubic-tetragonal transition, commonly observed in other perovskite ferroelectrics. On cooling, the cubic phase first transforms to two intermediate coexisting phases: (i) monoclinic (Pm) minority phase and (ii) tetragonal ($P4mm$) majority phase. While the intermediate tetragonal phase gradually disappears during cooling, the monoclinic phase, which is pseudotetragonal in nature with very large pseudotetragonality, transforms itself to a tetragonal phase with giant tetragonality over a large temperature interval ($450<T<680$ °C). The complex transition pathway of the system suggests that the structural transition is not driven primarily by soft ferroelectric mode of the system, if any. The formation of intermediate phases and the large temperature interval over which they evolve is suggestive of martenstic nature of this transition. The new transition pathway adopted by the system seems to be driven by the necessity to accommodate the extremely large spontaneous strain, which otherwise would not be possible in a single step cubic-tetragonal transition. For lower $BiFeO_3$ concentration ($x=0.40$ and 0.50) though the tetragonal phase observed at room temperature appears directly from the cubic phase, as in $PbTiO_3$, the x-ray powder-diffraction patterns of these compositions shows some of the features of the complex transition pathway. Thus the compositions $x=0.40$ and 0.50 have competing tendencies with regard to their phase transition behavior. In view of these results, it would be interesting to examine the transition pathways of other systems exhibiting giant tetragonality in the family of perovskite ferroelectrics.

ACKNOWLEDGMENTS

The authors thank the central x-ray diffraction facility of IISc for the high-temperature x-ray diffraction work, and Department of Science and Technology, India for financial support.

[1] B. Jaffe, W. R. Cook, and H. Jaffe, *Piezoelectric Ceramics* (Academic, New York, 1971).
[2] K. Uchino, *Ferroelectric Devices* (Marcel Dekker, New York, 2000).
[3] J. F. Scott and C. A. Araujo, Science **246**, 1400 (1989).
[4] F. Jona and G. Shirane, *Ferroelectric Crystals* (Pergamon Press, New York, 1962).
[5] S. A. Fedulov, P. B. Ladyzhinskii, I. L. Pyatigorskaya, and Yu. N. Venevetsev, Sov. Phys. Solid State **6**, 375 (1964).
[6] R. T. Smith, G. D. Achenbach, R. Gerson, and W. J. James, J. Appl. Phys. **39**, 70 (1968).
[7] V. V. S. Sai Sunder, A. Halliyal, and A. M. Umarji, J. Mater. Res. **10**, 1301 (1995).
[8] D. I. Woodward, I. M. Reaney, R. E. Eitel, and C. A. Randall, J. Appl. Phys. **94**, 3313 (2003).
[9] W.-M. Zhu, H.-Y. Guo, and Z.-G. Ye, Phys. Rev. B **78**, 014401 (2008).
[10] J. Chen, X. R. Xing, G. R. Liu, J. H. Li, and Y. T. Liu, Appl. Phys. Lett. **89**, 101914 (2006).
[11] S. Bhattacharjee, S. Tripathi, and D. Pandey, Appl. Phys. Lett. **91**, 042903 (2007).
[12] R. V. Shpanchenko, V. V. Chernaya, A. A. Tsirlin, P. S. Chizhov, D. E. Sklovsky, E. V. Antipov, E. P. Khlybov, V. Pomjakushin, A. M. Balagurov, J. E. Medvedeva, E. E. Kaul, and C. Geibel, Chem. Mater. **16**, 3267 (2004).
[13] J. Rodrigues-Carvajal, FULLPROF-2000. A Rietveld refinement and pattern matching analysis program, Laboratoire Leon Brillouin (CEA-CNRS), France.
[14] H. D. Megaw, *Crystal Structures: A Working Approach* (W. B. Saunders, London, 1973), p. 290.
[15] B. Noheda, J. A. Gonzalo, L. E. Cross, R. Guo, S.-E. Park, D. E. Cox, and G. Shirane, Phys. Rev. B **61**, 8687 (2000).
[16] A. K. Singh and D. Pandey, Phys. Rev. B **67**, 064102 (2003).
[17] R. Haumont, J. Kreisel, P. Bouvier, and F. Hippert, Phys. Rev. B **73**, 132101 (2006).
[18] P. Baettig and N. A. Spaldin, Appl. Phys. Lett. **86**, 012505 (2005).